Progress in Organic Coatings 112 (2017) 278–287

Contents lists available at ScienceDirect

Progress in Organic Coatings

journal homepage: www.elsevier.com/locate/porgcoat

A new corrosion protection approach for aeronautical applications combining a Phenol-paraPhenyleneDiAmine benzoxazine resin applied on sulfo-tartaric anodized aluminum

Alexis Renaud[a,*], Marc Poorteman[a], Julien Escobar[a], Ludovic Dumas[b], Yoann Paint[c], Leïla Bonnaud[c], Philippe Dubois[b], Marie-Georges Olivier[a]

[a] Department of Materials Science, Materials Engineering Research Center (CRIM), University of Mons, Place du Parc 20, B-7000 Mons, Belgium
[b] Laboratory of Polymeric and Composite Materials, Center of Innovation and Research in Materials and Polymers (CIRMAP), University of Mons, Place du Parc 20, B-7000 Mons, Belgium
[c] Materia Nova asbl, Avenue Copernic 1, B-7000 Mons, Belgium

ARTICLE INFO

Keywords:
Benzoxazine coating
Aluminum anodizing
Thermal curing
Barrier properties
Electrochemical impedance spectroscopy

ABSTRACT

In this paper, the feasibility to apply a laboratory synthesized Phenol-paraPhenyleneDiAmine (P-pPDA) benzoxazine by spin coating on anodized aluminum substrates followed by thermal curing, has been investigated. Prior to coating, sulfo-tartaric anodizing has been carried out aiming at growing porous oxide layers either on 1050 or 2024-T3 aluminum substrates.

Optimization of the performance of the benzoxazine coatings to protect the aluminum substrates was achieved by working out conditions preventing delamination of the coatings – as observed for non anodized coated substrates – and reducing its curing temperature to a level compatible with the requirements of the aerospace industry.

Compared to bare substrates coated with P-pPDA, it is shown that highly capacitive and durable barrier properties can be obtained for the same kind of coatings when applied on the anodized substrates. Moreover, in order to respect the thermal sensitivity of aeronautical aluminum substrates, such as 2024-T3, the curing temperature can be limited to 140 °C only if the substrates are previously anodized in a sulfo-tartaric acid bath.

1. Introduction

Aluminum alloys are widely used in aircraft applications, especially for series 2xxx (Cu main alloying element) and 7xxx (Zn main alloying element). These alloys offer improved mechanical properties compared to “pure” aluminum (AA1050), but are strongly sensitive to corrosion [1–3] and, therefore, need to be protected. For this purpose, a wide range of organic coatings has been developed and applied onto aluminum substrates providing a passive and/or active corrosion protection. Up to now, epoxy resins are the most commonly used thermoset polymers for such kind of applications [4,5].

Recently, polybenzoxazine resins have been reported to show several remarkable properties such as low water uptake, a high thermal stability, low shrinkage during curing [6] and a low dielectric constant [7]. These characteristics make them very suitable for coating protection applications [8,9]. However, those resins also suffer from some drawbacks, such as a high brittleness, a high curing temperature, and, in the case of bisphenol-based benzoxazine, an irreversible degradation occurring during curing, accompanied with the release of volatile imino species [8], causing severe defects to appear within the polymer (bubbles, cracks) reducing its reliability. Such defects can be avoided by selecting a more appropriate molecular design. Indeed, benzoxazine monomers are obtained by the simple condensation of formaldehyde, a phenol group and a primary amine, conferring a wide versatility to benzoxazine monomer compositions [10–13]. For instance, phenol-para-phenylenediamine based benzoxazine monomers (P-pPDA), have been recently reported in the literature [9,12,13] showing a higher thermal stability during curing leading to coatings with promising barrier properties. However, after several days of immersion in a NaCl solution, delamination processes at the metal/coating interface have been reported in the literature, leading to a loss of corrosion protection [9]. Another drawback related to this kind of benzoxazine is the high temperature needed for a complete crosslinking of the network. As shown previously [9], this temperature is higher than 220 °C and reduces the mechanical properties of aluminum alloys rich in copper, such as 2024-T3.

* Corresponding author.
E-mail address: alexis.renaud@umons.ac.be (A. Renaud).

http://dx.doi.org/10.1016/j.porgcoat.2017.07.007
Received 26 January 2017; Received in revised form 2 June 2017; Accepted 18 July 2017
0300-9440/ © 2017 Elsevier B.V. All rights reserved.

Table 1
Elementary chemical composition in weight percent of used aluminum alloys.

Alloy	Cu	Fe	Si	Mn	Mg	Cr	Zn	Ti	Others
1050	0.05	0.4	0.25	0.05	0.05	< 0.05	0.07	0.05	0.03
2024-T3	3.8 – 4.9	0.5	0.5	0.3 – 0.9	1.2 – 1.8	0.1	0.25	0.15	0.15

In order to reduce the risk of delamination, the P-pPDA organic coating was applied on an anodizing layer in this study. Anodizing is a surface treatment also used for improving the corrosion resistance of aluminum alloys. The process consists in an electrochemically driven growth of an oxide layer at the surface of the metal by applying an anodic potential. Performing this treatment in an acid bath allows the dissolution of the grown oxide. In the ideal case of pure aluminum, competition between growth and dissolution of the oxide leads to a particular ordered structure divided into two parts: a barrier layer in direct contact with the metal, and a porous layer of hexagonal columnar cells perpendicular to the substrate [14,15]. However, the presence of alloying elements such as copper may disturb this regular growth and lead to different oxide morphologies [16].

Chromic anodizing (in chromic acid electrolyte) has mainly been used as a very efficient and robust corrosion protection process [17]. However, because of health and environmental issues, such kind of treatment will be prohibited in the near future [18]. Alternative solutions have to be developed reaching aircraft standards related to health and environmental concerns. Other acid electrolyte baths have been investigated to replace chromic acid for these applications, such as sulfuric acid [19], sulfo-tartaric acid [20] or sulfo-boric acid [21]. In addition to the low cost of these substances, the combination of the strong sulfuric acid with the weak tartaric acid, limiting the oxide dissolution, offers a better control of the porosity without altering the conductivity of the electrolyte [22]. Oxide layers obtained from sulfo-tartaric baths have shown a better corrosion resistance compared to those obtained from classical sulfuric acid baths [23,24] and have already been accepted by the aerospace industry as an efficient alternative to a chromic acid bath. Sulfo-tartaric anodizing is usually performed at 37 °C under an applied potential difference of 14 V for about 20 or 30 min. The obtained layers have a thickness ranging from 2 to 7 μm [24,25].

In order to ensure a good corrosion protection, anodic layers can be sealed to obstruct the porosity of the layer. Hot water sealing is the simplest sealing bath [26–28], but several other types of baths containing additives have been studied and developed as reported in the literature [29–32]. When aluminum parts are intended to be painted in the final product, anodizing layers are not sealed but coated with a protective organic primer. As demonstrated at an industrial level, the anodic layer allows increasing the organic coating anchoring due to its high porosity. Nevertheless, there are few scientific papers reporting the improvement of the barrier properties of the global system due to this good matching between the inorganic layer and the organic one. The organic layer is commonly made of an epoxy resin, containing chromium trioxide as corrosion inhibitor [33]. Because of the content of this last toxic chemical in the epoxy layer, such kind of substances should be substituted as well. Several surface technologies are emerging as potential alternatives, such as sol-gel coatings [34–36] and new polymeric organic coatings [37–40].

This work proposes, as an alternative for epoxy coatings, a new corrosion protection system where P-pPDA benzoxazine is coated on anodized aluminum substrates with the aim of limiting delamination processes occurring after application on not anodized surfaces offering more durable barrier properties. In order to emphasize the role of the anodic layer in the prevention of the loss of the barrier properties, equivalent thickness coatings of P-pPDA have also been applied on bare substrates and characterized to be compared with coatings on anodized aluminum.

The substrate of interest in this paper is AA2024-T3, containing copper as the main alloying element, which enhances the mechanical properties, and, for this reason, is mainly used in the aircraft industry. However, this kind of substrate needs to be covered by a protecting system showing good barrier properties and, at the same time, avoiding curing at too high temperatures. For this reason, part of the study has also been devoted to assess the barrier performance of partially cured P-pPDA benzoxazine, applied on either bare or anodized substrates. However, AA2024-T3 substrates can also be used with a clad deposit of AA1050 on top of its surface in order to improve its corrosion protection. Therefore, both kinds of alloys have been investigated as substrate materials.

2. Experimental

2.1. Preparation process of aluminum substrate

Two aluminum alloys, provided by SONACA S.A. (Gosselies, Belgium) have been selected: AA1050 and AA2024-T3. Details of their chemical compositions are in Table 1.

Aluminum samples (60 mm × 45 mm × 1 mm) were treated prior to anodizing in order to enable the formation of a homogeneous oxide layer. The different steps are: degreasing in acetone, etching in 1 M NaOH at 40 °C for 1 min, desmutting in Turco® Liquid Smut-Go NC Deoxidizer at room temperature for 15 s with rinsing in deionized water between each step.

Anodizing of samples in a sulfo-tartaric bath was carried out using the following concentrations: 40 g/L H_2SO_4 + 80 g/L $C_4H_6O_6$. The bath temperature was controlled using an outer water flow with set temperature. A fixed anodizing potential difference was applied using a Laboratory Power Supply EA Elektro-Automatik PS-2016-100. Anodizing parameters have been fixed as follows: bath temperature at 40 °C and applied potential difference at 10 V for 25 min. Those settings are close to the ones commonly used in the industry [25].

After pretreatment and subsequent anodizing, samples were rinsed in deionized water, dried with pulsed air and directly coated with an organic solution of benzoxazine precursor in chloroform. This solution was prepared by dissolving 8 g of P-pPDA-benzoxazine precursor (Fig. 1) – synthesized as described in a previous paper [13] – in 40 mL of chloroform, stirring and heating under reflux for 4 h at 70 °C followed by cooling down to room temperature, maintaining stirring for 12 h. This solution was applied on substrates by deposing 1 mL on the samples, spin coated at 2000 rpm for 30 s.

After deposition and drying of the precursor coating, thermal curing

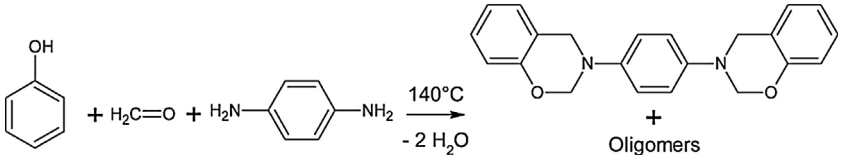

Fig. 1. One pot synthesis of P-pPDA precursor.

was carried out stepwise to obtain a cross-linked polymer by successive thermal curing steps: at 140 °C for 60 min, 180 °C and 220 °C, with each time a dwell of 120 min, and, finally, at 230 °C for 30 min. Afterwards, samples were allowed to slowly cool down to room temperature. This curing cycle corresponds to the standard crosslinking treatment of the resin [9], and will be called standard (Std) in this article. Other thermal treatments with lower curing temperatures were also performed and will be detailed later. The samples were thermally treated in a Heraeus Instruments LUT 6050 oven in horizontal position to avoid outflow and loss of benzoxazine during the treatment.

2.2. Characterization

2.2.1. Textural analysis of anodized and coated samples

Anodized and coated samples were observed using SEM-FEG (Hitachi SU8020 with cold cathode) without metallization. Cross section observations were performed by cutting samples using cryogenic breaking: after one minute immersion in liquid nitrogen, samples were clamped and bent to rupture. Using Image J 1.48 v software, the thickness of the polymer layers has been measured on SEM-FEG micrographs. Thickness and pore size of oxide layers have been measured from the SEM-FEG surface and cross-section micrographs respectively, whereas the surface porosity has been obtained from area calculation on surface micrographs treated to binary pictures using Image J 1.48 v software.

2.2.2. Electrochemical properties and modeling

A conventional three-electrode cell was used for the electrochemical tests. The working electrode was the investigated sample (exposed area of 7.07 cm^2), the counter electrode was a platinum plate and all potentials were measured with respect to an Ag/AgCl/Satured KCl (+0.197 V vs SHE) reference electrode. The cell was placed in a Faraday cage in order to minimize external electromagnetic interference on the system. The impedance measurements were carried out over frequencies ranging from 100 kHz to 10 mHz, at ambient temperature. The impedance spectra were acquired by using a potentiostat coupled with a frequency response analyser (Parstat 2273 from Ametek), computer-controlled with Powersuite® software. Electrochemical impedance measurements were performed after different immersion times in 0.1 M NaCl solution on the different systems. The signal amplitude was 30 mV rms. Three samples of each type have been characterized in order to check the reproducibility of the EIS results. The presented EIS spectra correspond to the representative behavior of each type. Impedance measured data have been fitted using equivalent electrical circuits. The impedance values of electrical components have been iterated to fit experimental impedance data using a fitting software: ZSimpWin 3.50.

2.2.3. Determination of the solvent resistance

The chemical resistance of the organic coatings, which is related to the cross-linking of the resin, has been assessed by solvent rubs using methyl ethyl ketone (MEK) according to ASTM D5402 standard.

2.2.4. Glass transition temperature and crosslinking degree estimation

Calorimetric studies were carried out at a heating rate of 10 °C/min from 0 up to 315 °C using a differential scanning calorimeter (DSC Q200 from TA Instruments) under nitrogen flow of 50 mL/min. An Indium standard was used for calibration.

3. Results and discussion

3.1. Morphology of anodic oxide layers

Fig. 2a and b show the surface and a cross-section respectively of an anodic film obtained on AA1050 after 25 min of anodizing in a sulfotartaric acid bath at 40 °C under 10 V. It can be observed that the oxide layer shows a homogeneous thickness of about 3 µm, comparable to those usually reported in the literature [24] and following the roughness of the substrate.

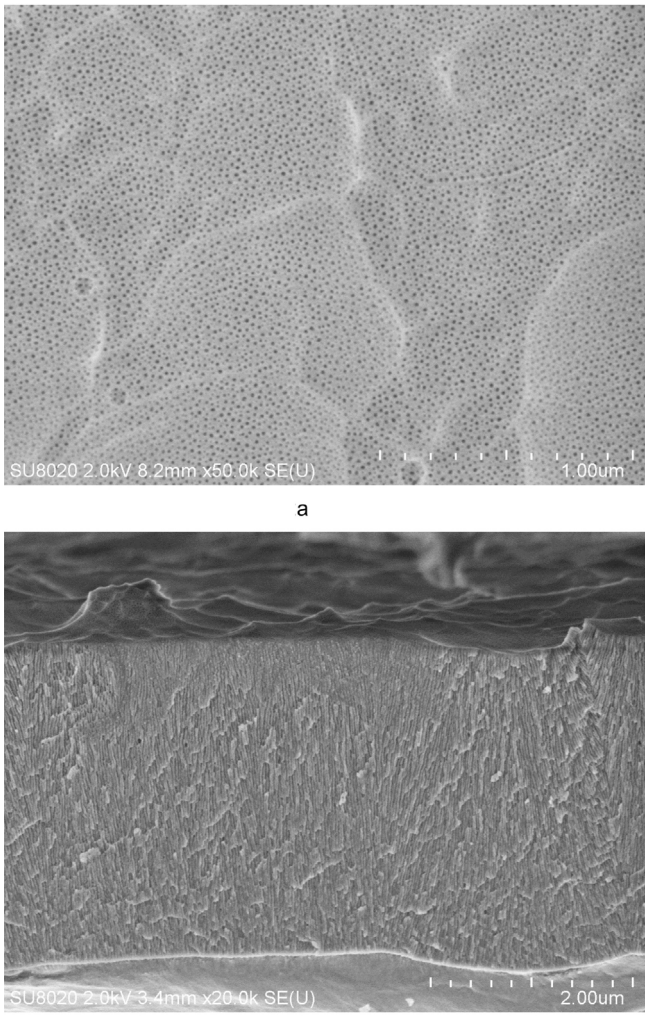

Fig. 2. SEM-FEG micrographs of the a) surface (×50,000) and the b) cross-section (×20,000) of the oxide layer on AA1050 obtained from anodizing at 10 V for 25 min in a bath at 40 °C.

The influence of the substrate composition on the anodic layer has been studied. Fig. 3a and b show the surface and cross-section of an anodic film obtained on AA2024-T3 under the same anodizing conditions as previous (25 min, 40 °C and 10 V). A difference in oxide morphology, compared to the layer obtained on AA1050 can clearly be observed in Fig. 2a and b. Effectively, anodic layer surfaces on AA2024-T3 present several defects and micron sized pores, which can be attributed to the presence of copper-rich intermetallic particles and the dissolution of grain boundary precipitates [41]. From the cross section micrograph, it can be observed that the tubular structure of the nanopores, as in anodized AA1050, is not present in anodized AA2024-T3 and is replaced by a sponge-like morphology, explained by the generation of oxygen gas at copper-rich sites during anodizing [16]. However, despite this visual difference, oxide layers on AA1050 and AA2024-T3 appear to have very similar characteristic dimensions, as detailed in Table 2.

3.2. Morphology of Std cured P-pPDA coating on oxide layers

The thickness of the deposited organic layer was estimated from

a

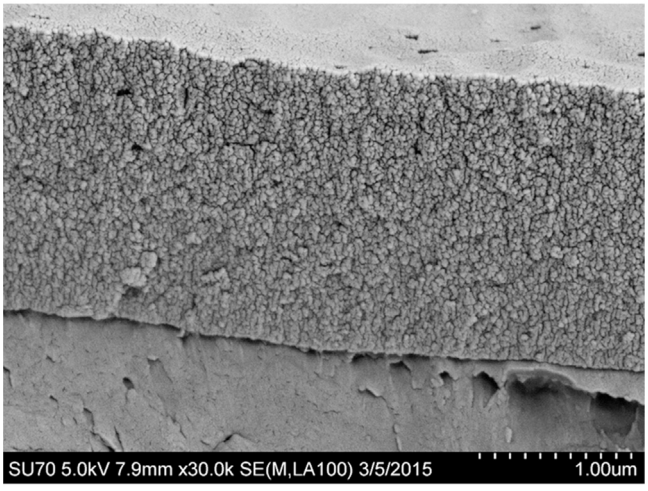

b

Fig. 3. SEM-FEG micrographs of the a) surface (×50,000) and the b) cross-section (×30,000) of the oxide layer on AA2024-T3 obtained from anodizing at 10 V for 25 min in a bath at 40 °C.

Table 2
Anodic layers characteristics obtained on AA1050 and AA2024-T3 with the same anodizing settings (10 V at 40 °C for 25 min).

Substrate	Thickness (μm)	Pore diameter (nm)	Surface porosity (%)
AA1050	3.2 ± 0.1	12.9 ± 1.6	12.3
AA2024-T3	2.8 ± 0.1	12.2 ± 2.0	17.1

SEM-FEG micrographs of P-pPDA coated on different anodized aluminum substrates (AA2024-T3 and AA1050). The measured average thickness of the Std cured P-pPDA coating is 2 μm ± 0.2 μm in both cases.

The interface between the organic coating and the oxide layer after curing was observed using SEM-FEG. Fig. 4a and b show cross-section SEM-FEG micrographs of cured P-pPDA coatings on anodized AA1050 and AA2024-T3 alloys respectively. From these pictures, a uniform coverage of the organic layer all over the oxide surface is observed at micrometric scale. The interface between organic and anodic layers seems to be even more cohesive when obtained on AA2024-T3 substrates. The surface of the anodic layer obtained on AA2024-T3 appears to be rougher, even at nanometric scale, probably providing a higher interaction area compared to AA1050 enabling some penetration of P-pPDA through the pores in favor of a more cohesive interface.

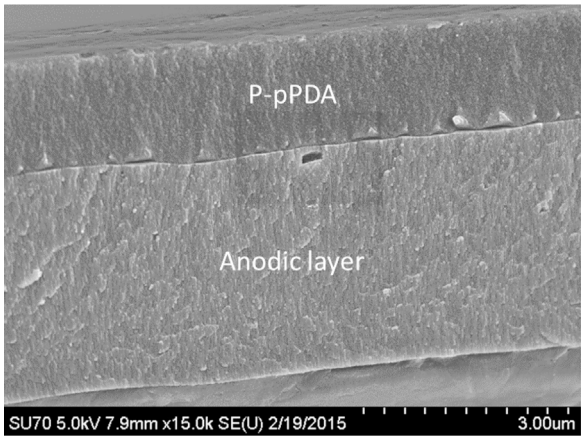

a

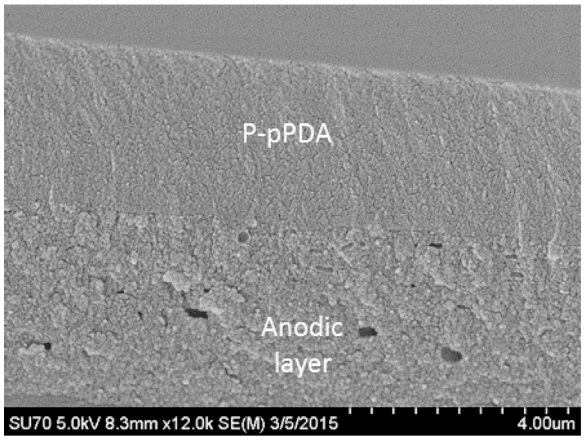

b

Fig. 4. SEM-FEG micrographs of the cross-section of P-pPDA coated (Std curing) on anodized AA1050 (a) and anodized AA2024-T3 (b) (anodizing settings: 10 V, 25 min, 40 °C).

3.3. Electrochemical behavior of P-pPDA coated on aluminum cured with the standard temperature cycle

3.3.1. EIS of P-pPDA coated aluminum without anodic layer and Std cured

Fig. 5a and b shows the evolution of the EIS spectrum over immersion time obtained from EIS on pretreated, but not anodized, A-A1050 and AA2024-T3 respectively, each coated with P-pPDA and cured using the standard treatment. At the initial time of immersion, the coatings show very good barrier properties, with high time constants covering a large range of frequencies and values of the impedance modulus at low frequency (estimation of the resistance of the system) of the order of $10^{7} \sim {}^{8}$ Ohm cm^2. However, after one week of immersion, this last value has already decreased of one order of magnitude. After several days of immersion, the time constant corresponding to the coating becomes narrower and a second time constant appears in the impedance phase plot at lower frequencies, witnessing of delamination and corrosion processes taking place at the metal/coating interface. Impedance data can be fitted using the equivalent electrical circuit presented in Fig. 6 where R_p and Q_c represent the resistance of the pores and the capacitance of the coating respectively. R_{ox} and Q_{ox} are the resistance and the capacitance respectively of the oxide layer at the surface of the substrates. R_{ct} and Q_{dl} are the charge transfer resistance and the double layer capacitance at the electrolyte/metal interface, respectively. However, the strong scattering of the impedance data points at low frequencies results in a poor accuracy of the fitted impedance for this last time constant. Thus, this time constant has not

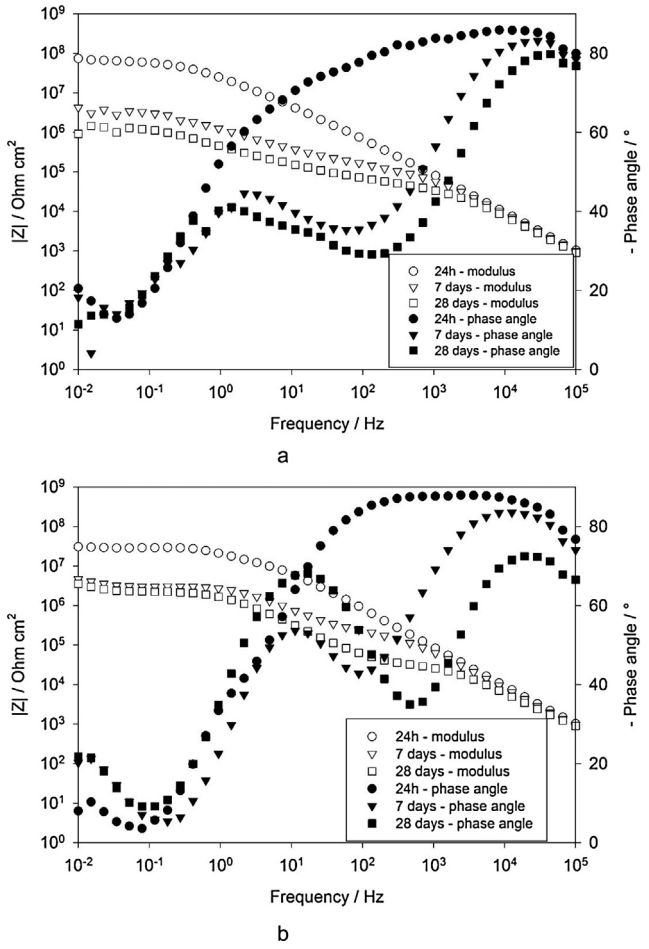

Fig. 5. Evolution of EIS spectra over immersion time in 0.1 M NaCl electrolyte of P-pPDA coated (Std curing) on bare AA1050 (a) and AA2024-T3 (b).

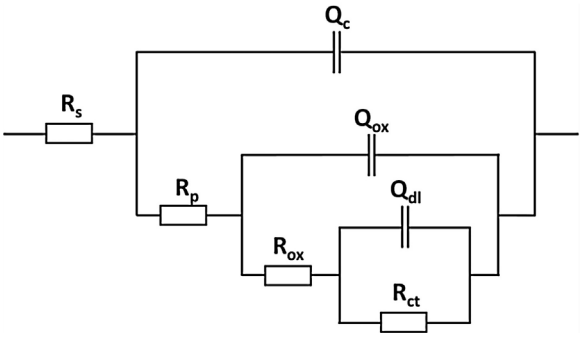

Fig. 6. Equivalent electrical circuit used to fit impedance data of P-pPDA coated on bare aluminum substrates.

been considered and the impedance data points of the lowest frequency decade have been excluded from the fitting procedure. R_s represents the resistance of the electrolyte, which is about 1 10^2 Ohm cm^2. Constant Phase Elements (CPE) were used instead of pure capacitances in order to take into account the non-ideal behavior of the organic layer and the electrochemical double layer. In the literature, the impedance of a constant phase element is written as $Z_Q = 1/Y_0(i\omega)^{-n}$ where Y_0 is the CPE admittance and the CPE exponent n is the frequency dispersion factor varying from 0 to 1. If n = 0, the CPE behaves as a resistor. If n = 1, the CPE is a pure capacitance [42]. In this case, n is higher than 0.9, reflecting a very capacitive behavior. Fig. 7 compares the evolution of the calculated pores resistance R_p and coating capacitance Q_c (with corresponding n values) for coatings applied on bare AA1050 and on

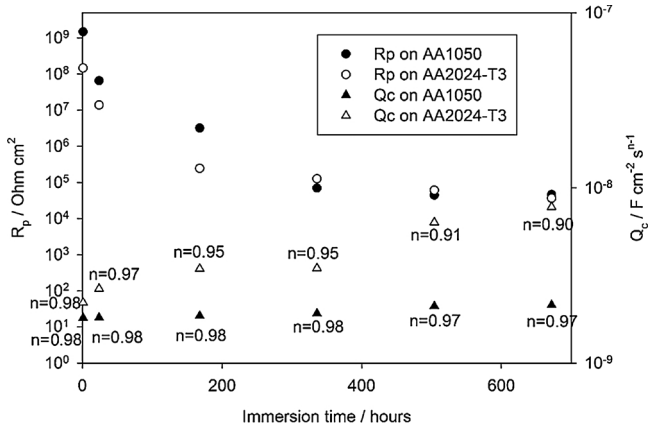

Fig. 7. Evolution of the calculated pores resistance R_p and coating capacitance Q_c (with corresponding n values) over immersion time in 0.1 M NaCl electrolyte for P-pPDA coatings (Std cured) applied on bare aluminum substrates.

bare AA2024-T3. The values of the resistance determined for the two substrates are high at initial immersion time for a coating having a thickness of 2 µm (more than 1 10^8 Ohm cm^2) and so the systems initially act as good barriers. However, these values strongly decrease down to 10^4 Ohm cm^2 at the end of the immersion period. Concerning the coating capacitances, it can be observed that this value is very slowly increasing in the case of coatings on bare AA1050 substrates (with very slight changes in n value as well), whereas it exhibits a significant increase in the case of coatings on bare AA2024-T3, accompanied with a decrease of the n value down to 0.90. Such evolutions in Q_c and n values are confirming the occurrence of delamination processes at the metal/coating interface and/or degradation of the coating integrity. Indeed, it seems difficult to relate the capacitance increase over days of immersion to water uptake, since this phenomenon occurs during the first hours of immersion. The water uptake of the same resin coatings has already been calculated using Brasher & Kingsbury equation in a previous paper [9] where it was estimated to be lower than 1%. For longer immersion times, an increase in the capacitance value, accompanied by a decrease in n factor, is then rather attributed to the delamination and/or the degradation of the coating [43–45]. A comparable behavior has also been observed for a thicker layer of P-pPDA and explained more deeply in a previous study [9] which was only related to an AA1050 substrate. The same behavior of the pore resistance versus immersion time is observed for both alloys, whereas the higher reactivity of AA2024-T3 substrates appears to lead to a faster delamination and/or degradation rate of the coating, explaining the stronger increase in Q_c values and decrease in n values compared to AA1050 substrates and the corresponding n decrease.

3.3.2. EIS of P-pPDA coated aluminum with anodic layer and Std cured

Fig. 8a and b shows the evolution of impedance plots over immersion time obtained from EIS on anodized AA1050 and anodized A-A2024-T3 respectively (settings: 10 V, 40 °C, 25 min) each coated with P-pPDA and, again, Std cured. During the first hour of immersion, the impedance moduli at low frequency are higher than 10^9 Ohm cm^2, and one time constant covers the whole range of frequencies from 0.01 Hz to 10^5 Hz. For longer immersion periods, even after 28 days and for both alloys, the impedance modulus at low frequency stays very high (over 10^9 Ohm cm^2) and the absolute value of the phase angle remains higher than 70° in the whole range of frequencies. This electrochemical behavior highlights the excellent barrier properties of anodized and coated systems, showing a big improvement in terms of resistance, capacitance and durability compared to organic or anodic layers alone. Indeed, unsealed anodic layers obtained by sulfo-tartaric anodizing on AA1050 have already been characterized by EIS in a previous study [46], exhibiting a less capacitive behavior in the investigated frequency

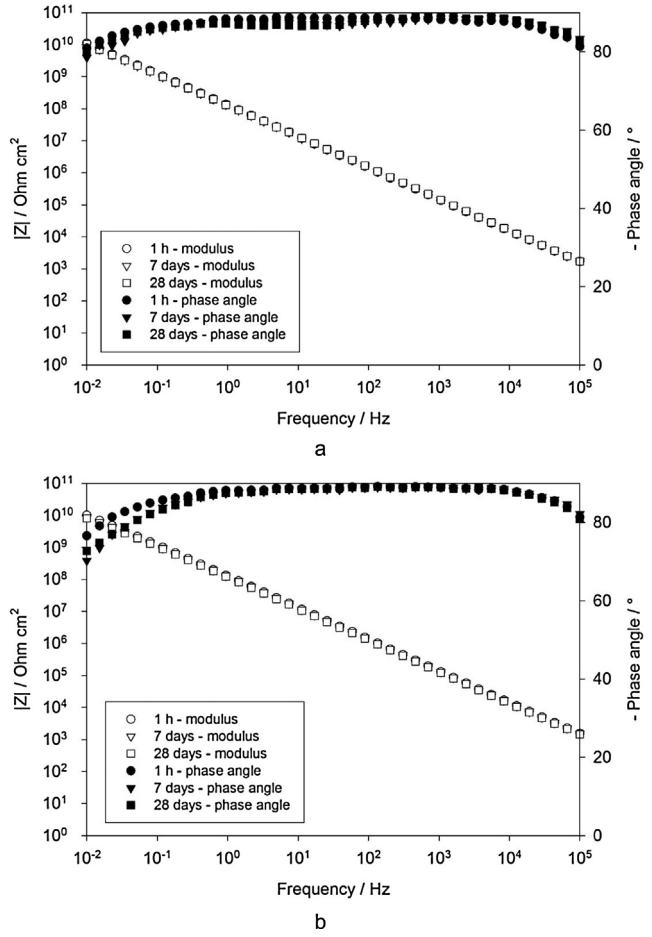

Fig. 8. Evolution of EIS spectra over immersion time in 0.1 M NaCl electrolyte of P-pPDA coated (Std curing) on anodized AA1050 (a) and anodized AA2024-T3 (b) (anodizing settings: 10 V, 40 °C, 25 min).

range, a lower impedance modulus at low frequency (inferior to 10^7 Ohm cm^2 at the beginning of immersion) and less stable behavior with immersion time. In the case of unsealed anodized AA2024-T3, corrosion starts in the first hours of immersion.

The higher impedance modulus at low frequency could be explained by the higher total thickness (3 µm of oxide + 2 µm of coating) of anodized and coated systems compared to clear coatings (only 2 µm), and by the fact that the electrolyte does not fill the porous part of the anodic layer as it is obstructed by the resin. The improvement of durability is likely to be related to the favorable interaction between organic and anodic layers. Indeed, the high surface roughness of the oxide as observed from SEM-FEG pictures (3.2) leads to an improved cohesion between the polymer layer and the anodic layer, therefore preventing or limiting delamination processes.

When looking in more detail to the phase angle diagram in the case of P-pPDA coated on anodized AA1050 (Fig. 8a), we can distinguish a local minimum in the mid frequency range. Indeed two strongly overlapping time constants can be distinguished whereas the value of the modulus at low frequency remains very high (10^{10} Ohm cm^2). This original electrochemical behavior might be associated to the formation of resistive pathways through the organic layer where the electrolyte can pass and finally reach the anodic layer. The slightly resistive tendency in the mid frequency range is then attributed to these resistive pathways through the resin layer, while the fully capacitive behavior observed from mid to high frequency range is associated to the capacitance of the two superimposed organic and anodic layers. The second time constant in the low frequency range could be attributed to the anodic layer reached by the electrolyte through the organic layer. Since

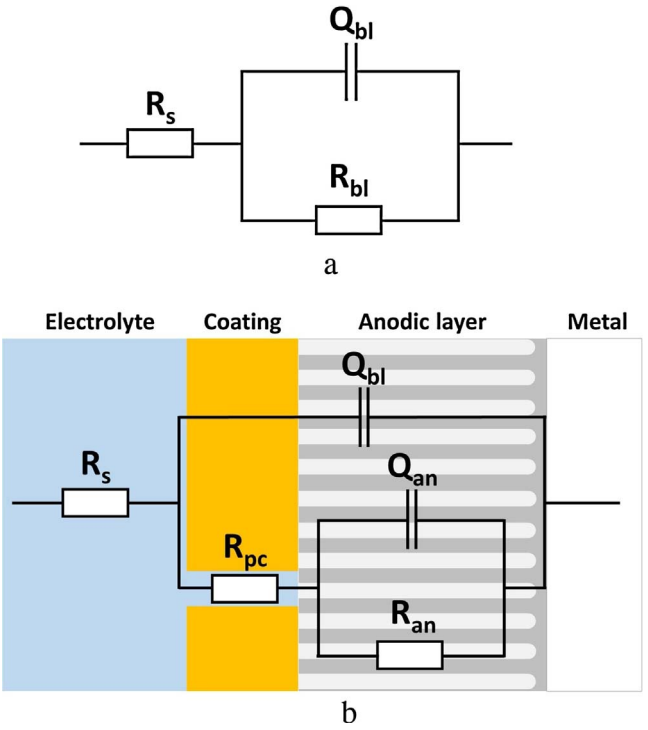

Fig. 9. Equivalent electrical circuit used to fit impedance data of P-pPDA coated on anodized AA1050 after one day (a), one week (b) and one month (b) of immersion in 0.1 M NaCl electrolyte.

the porous part of the oxide layer has not been sealed, the contribution of the barrier layer is expected to be predominant.

The impedance data have been fitted in order to evaluate the different resistive and capacitive behaviors. The EEC displayed in Fig. 9a has been used for fitting impedance data at initial time of immersion, where R_s is the resistance of the electrolyte, and Q_{bl} and R_{bl} are the capacitance and the resistance of the bi-layer respectively. A CPE is used to take into account the non-ideal behavior of the system. For one week and one month of immersion, impedance data have been fitted using the EEC presented in Fig. 9b, where Q_{bl} is the capacitance of the bi-layer (a CPE is used as well), R_{pc} is the resistance of the pores through the resin coating, and Q_{an} and R_{an} the capacitance and the resistance of the anodic layer respectively. The exact EEC corresponding to this system should probably be more complex, especially concerning the anodic layer. For example, diffusion phenomena are likely to be involved in the columnar pores of the anodic layer. A partial and progressive sealing of the pores by hydration of the alumina could also be expected as it has already been shown [46]. Two time constants are commonly used to model the electrochemical properties of such layers [46]. However, because of the strong overlapping of the time constants, the contribution of the porous and barrier parts of the oxide layer could not be separated. The global contribution of those two parts of the spectra have then been included in one single time constant (Q_{an} and R_{an}) where the use of a CPE reflects the complex behavior of the anodic film. The results of the impedance data fitting are shown in Table 3. After one week and one month of immersion, the resistance of the coating pores (R_{pc}) is of the order of 10^7 Ohm cm^2, which is significantly higher compared to the resistance obtained on bare aluminum for an equivalent immersion time (order of 10^4 Ohm cm^2). Even though the anodic layer cannot completely prevent resistive pathways to appear and propagate, it seems to limit this phenomenon and its impact on the barrier properties. Concerning the parameters of the time constant associated with the anodic layer, the value of n is around 0.8, illustrating the complex electrochemical behavior of this layer. A very low capacitance (order of 10^{-10} F cm^{-2} s$^{(n-1)}$) and a very high

Table 3
Results of the fitting of the impedance data obtained by EIS measurements on cured P-pPDA coated on anodized AA1050 after one hour, one week and one month of immersion using EECs displayed in Fig. 9.

Immersion time	Q_{bl}	n_{bl}	R_{bl}	–	–	–
	$nF\ cm^{-2}\ s^{(n-1)}$		$GOhm\ cm^2$			
1 hour	1.28	0.98	77.6	–	–	–
–	Q_{bl} $nF\ cm^{-2}\ s^{(n-1)}$	n_{bl}	R_{pc} $MOhm\ cm^2$	Q_{an} $nF\ cm^{-2}\ s^{(n-1)}$	n_{an}	R_{an} $GOhm\ cm^2$
1 week	1.19	0.98	33.7	0.15	0.79	80.5
1 month	1.18	0.99	90.3	0.17	0.81	104

resistance (order of $10^{10} \sim^{11}$ Ohm cm^2) are obtained for the oxide layer. In the literature [46] values of the order of 10^{-7} F cm^{-2} $s^{(n-1)}$ for the capacitance and $10^7 \sim^{8}$ Ohm cm^2 for the resistance are obtained for anodic layers. This difference is easily explained by the fact that in our case the area of anodic layer analyzed by the EIS measurements is only the oxide area reached by the electrolyte through the resin coating, whereas the whole anodic layer area is characterized in the case of uncoated samples. This area ratio leads to much lower capacitance values and higher resistance values. For anodized AA2024-T3 substrates coated with P-pPDA, this kind of evolution is not observed. When fitting impedance data of this system using the EEC of Fig. 9a, values of about 1.3 10^{-9} F cm^{-2} $s^{(n-1)}$ for Q_{bl} (with n = 0.98) and about 4 10^{10} Ohm cm^2 for R_{bl} are obtained over the whole immersion time. This longer durability can be attributed to the rougher surface of the oxide layer, providing a stronger anchoring of the resin and preventing the propagation of resistive pathways and delamination. The presence of copper in the alloy, which is the reason for its poor corrosion resistance as a bare substrate, leads to a much favorable morphology of the oxide layer as an anodized substrate, offering more durable barrier properties.

3.4. Reducing the curing temperature

3.4.1. Reduced curing of coated bare aluminum

AA2024-T3 aluminum alloy cannot withstand a too high temperature for a long time without losing its high mechanical properties. This mechanical failure is attributed to the modification of hardening precipitates from θ' phase, having a semi-coherent interface with the aluminum matrix, to θ phase having an incoherent interface with the matrix [47]. Therefore, the long and high temperature Std curing cycle of P-pPDA is not compatible with the thermal sensitivity of the AA2024-T3 substrate for aeronautical applications. In order to avoid the deterioration of the mechanical properties of the alloy, a partial curing of the resin at lower temperatures has been considered. Three new curing cycles with limited curing temperature have been compared in order to emphasize the relevance of a partial curing of the coating. Table 4 sums the alternative curing cycles and corresponding ASTM D5402 results, estimated glass transition temperature and crosslinking degrees obtained by DSC. For a complete curing, the Tg value reaches 215 °C and decreases down to 125 °C for the curing cycle performed at 140 °C. The results confirm that only a partial curing is obtained for each of the selected cycles. The lowest crosslinking degree obtained at 140 °C is around 50%. In order to check that a sufficient degree of cross-linking was achieved with each partial curing cycle, the solvent resistance of benzoxazine coatings applied on AA1050 were determined by using the MEK test. For all curing cycles, coatings endure 100 double-rubs, whereas non-cured coatings are dissolved after only 14 double-rubs. Therefore, all partially and fully cured coatings exhibit a high solvent resistance and consequently sufficient cross-linking degree.

Partially cured coatings with a thickness of 2 µm of P-pPDA have been applied on bare aluminum substrates and characterized using EIS in a 0.1 M NaCl electrolyte. Because of the too high reactivity and corrosion rate of bare AA2024-T3 substrates immersed in saline solutions, AA1050 substrates have first been preferred for EIS measurements in order to limit the corrosion and focus on the coating behavior. Indeed, for coatings applied on bare AA2024-T3 and cured with different partial curing cycles, corrosion started on all samples after a few hours of immersion, offering no interesting comparison of the coatings barrier properties regarding the curing degree. Fig. 10 shows the comparison of impedance plots obtained by EIS from coatings cured with different cycles. All coatings appear to have very similar electrochemical behavior at the beginning of the immersion in the saline electrolyte solution. However, electrochemical properties evolve differently depending on the curing temperature of the applied coating. In order to follow and compare the evolution of electrochemical properties of the coatings, impedance data have been fitted using the Equivalent Electrical Circuit shown in Fig. 6. Again, n values were higher than 0.9. Fig. 11 compares the evolution of the pores resistance R_p and coating capacitance Q_c over immersion time for all coatings. A significant decrease in R_p is observed for all coatings, while Q_c remains stable. At the initial immersion time, coatings cured at 180 °C and Std curing cycles show the highest R_p values of about 3 10^{10} Ohm cm^2. However, the coating cured following the standard curing cycle presents the strongest decrease in R_p and drops down to values lower than 10^3 Ohm cm^2. Coatings cured using curing cycles at 140 °C or 160 °C show similar behavior for long times of immersion (more than two weeks) despite a significant difference of more than one order of magnitude during the first days of immersion. Finally, the coating cured using the 180 °C curing cycle shows the lowest decrease in R_p and keeps values higher than 10^8 Ohm cm^2.

These results show that, regarding barrier properties and their durability, an optimal curing temperature exists. Indeed, in order to

Table 4
Curing cycles and corresponding solvent resistance (ASTM D5402).

Curing cycle	Designation	Glass transition temperature (°C)	Crosslinking degree (%)	Double-rubs endured
1 h at 140 °C + 2 h at 180 °C + 2 h at 200 °C + 30 min at 220 °C + 30 min at 230 °C	Standard (Std)	215	100	100
1 h at 140 °C + 4 h at 180 °C	180 °C	185	93	100
1 h at 140 °C + 4 h at 160 °C	160 °C	166	70	100
5 h at 140 °C	140 °C	125	48	100
No curing	–	–	0	14

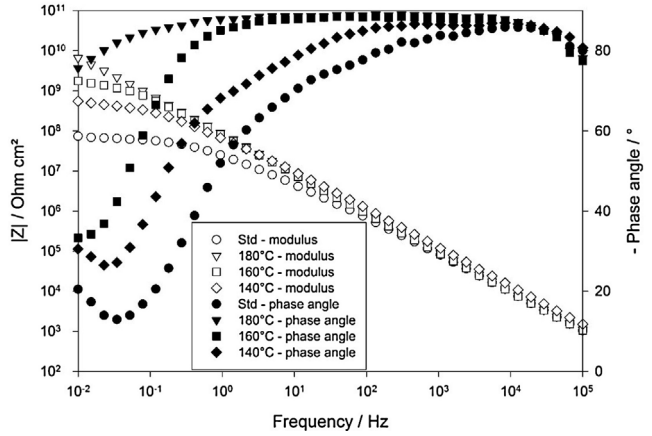

Fig. 10. Comparison of EIS spectra obtained on bare AA1050 coated with P-pPDA cured with four different cycles after one day of immersion in 0.1 M NaCl electrolyte.

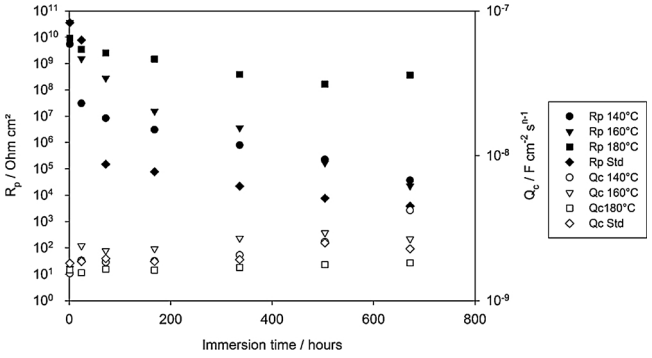

Fig. 11. Evolution of the calculated pores resistance R_p and coating capacitance Q_c over immersion time in 0.1 M NaCl electrolyte for coatings of P-pPDA coated on bare AA1050 and cured with four different cycles (CPE: n > 0.9).

present high barrier properties, the crosslinking degree should be high enough (around 90%). On the other side, if the crosslinking degree is too high, mechanical stresses are likely to be higher at the coating substrate interface due to the thermal expansion mismatch between both materials and to the fact that these stresses are less dissipated in a more rigid polymer. The observed optimum can then be attributed to the existence of a good compromise between the crosslinking degree of the coating on the one side and the limitation of the mechanical stresses generated in the coating and at the interface with the substrate during the curing process on the other side, leading to an efficient and cohesive barrier. This optimal curing temperature is close to 180 °C, which is slightly too high for the targeted application.

3.4.2. Reduced curing of coated anodized aluminum

The same kind of experimental investigation has been performed on anodized substrates. Coatings of P-pPDA with a thickness of 2 µm have been applied on AA1050 and AA2024-T3 anodized at 40 °C under 10 V for 25 min. EIS spectra of anodized substrates coated with P-pPDA cured with the four different curing cycles are shown at initial and final immersion times on AA1050 and AA2024-T3 as shown in Figs. 12 and 13 respectively. All systems exhibit very similar behavior. At initial immersion time, EIS spectra are almost exactly superimposed regardless the curing degree, and this strong similarity is observed on both alloys.

In the case of anodized AA1050, the distinction of two time constants after one month of immersion is observed for all curing cycles except for curing at 180 °C. This exception is in accordance with the optimal barrier properties observed for this curing cycle on bare substrates. P-pPDA coatings cured with this thermal treatment do not appear to suffer from any appearance or propagation of resistive pathways over immersion time, leading to enhanced barrier properties and

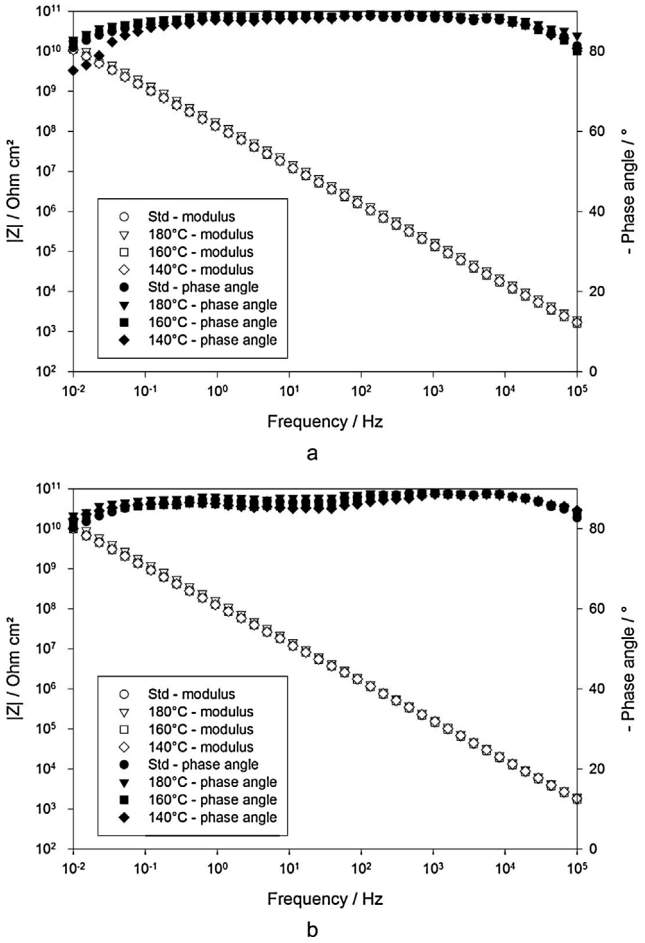

Fig. 12. Comparison of EIS spectra obtained on anodized AA1050 coated with P-pPDA cured with four different cycles after one hour (a) and one month (b) of immersion in 0.1 M NaCl electrolyte.

durability.

On anodized AA2024-T3, it can clearly be observed that all EIS spectra are almost exactly superimposed at initial and final immersion times. Comparable, highly capacitive and durable properties appear to be obtained regardless the applied curing cycles. For coatings applied on anodized AA2024-T3, partial curing can therefore be used for obtaining protective coating systems, without loss in barrier properties, and this is likely to be related to the cohesive interface between the organic coating and the oxide porous layer.

4. Conclusions

Phenol-paraPhenyleneDiAmine-based benzoxazine has been successfully spin-coated and, first, cured at 230 °C on anodized AA1050 and AA2024-T3 substrates. The nano-porous morphology of anodic layers obtained from sulfo-tartaric anodizing enhances the interaction surface with this new kind of organic resin. Such an improved interface promotes adhesion and prevents delamination processes to occur at the interface between the anodized layer and the benzoxazine layer. Therefore, the electrochemical properties of this system appear to be highly capacitive and more durable for periods of over one month of immersion in 0.1 M NaCl electrolyte whereas the organic coating thickness is limited to only 2 µm.

Moreover, P-pPDA coatings applied on anodized AA2024-T3 – known for its high mechanical properties but high corrosion sensitivity – exhibited an even more durable behavior, explained by the additional micro and nano-porosity of the anodic layer for this alloying composition, leading to an even more cohesive interface between the coating

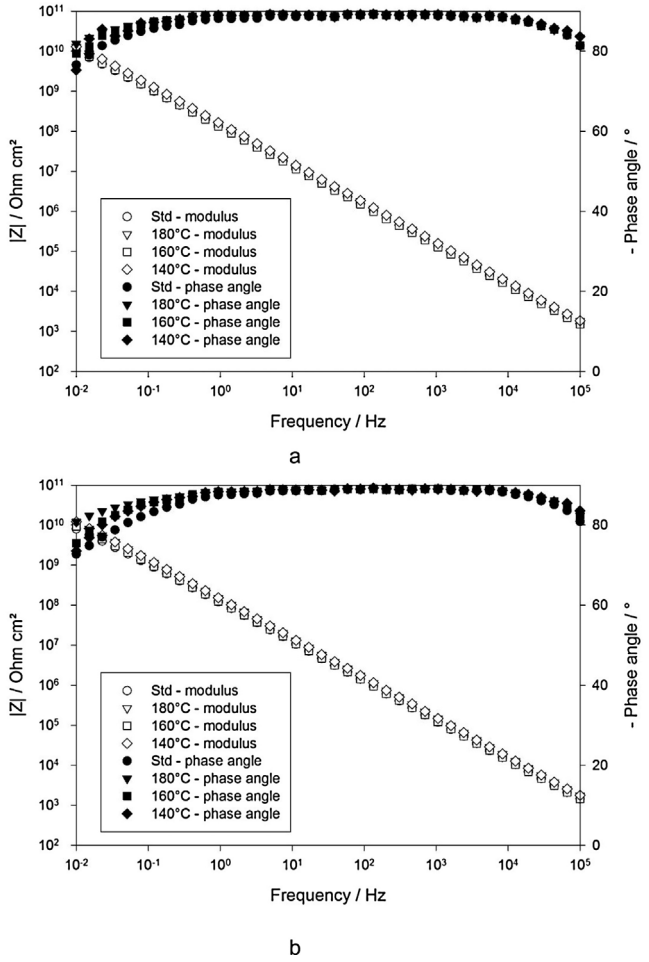

Fig. 13. Comparison of EIS spectra obtained on anodized AA2024-T3 coated with P-pPDA cured with four different cycles after one hour (a) and one month (b) of immersion in 0.1 M NaCl electrolyte.

and the oxide.

In order to respect the thermal sensitivity of the AA2024-T3 substrate, curing cycles at lower temperatures than 230 °C have been used leading to partially cured P-pPDA coatings applied on both bare and anodized substrates. On bare substrates, an optimal curing temperature has been identified around 180 °C. Interestingly, on anodized substrates, all curing cycles led to highly capacitive and durable electrochemical properties of the system, offering a wider range for adapting the curing process of the resin, for instance to the substrate properties.

Acknowledgments

The authors wish to thank the “Région Wallonne” in the framework of the “Programme d’Excellence: OPTI²MAT and FLYCOAT” and the FEDER 2014–2020 program: HYBRITIMESURF. Finally, the authors wish to thank SONACA for providing aluminum samples.

References

[1] N. Murer, R. Oltra, B. Vuillemin, O. Néel, Numerical modelling of the galvanic coupling in aluminium alloys: a discussion on the application of local probe techniques, Corros. Sci. 52 (2010) 130–139.
[2] A.-P. Romano, M.-G. Olivier, A. Nazarov, D. Thierry, Influence of crosslinking density of a cataphoretic coating on initiation and propagation of filiform corrosion of AA6016, Prog. Org. Coat. 66 (2009) 173–182.
[3] Geraint Williams, Andrew J. Coleman, H. Neil McMurray, Inhibition of Aluminium Alloy AA2024-T3 pitting corrosion by copper complexing compounds, Electrochim. Acta 55 (2010) 5947–5958.
[4] A. Foyet, T.H. Wu, A. Kodenstov, L.G.J. van der Ven, G. de With, R.A.T.M. van Benthem, Absorption of water and corrosion performance of a clear and pigmented epoxy coating on Al-2024 alloy, ECS Trans. 29 (29) (2010) 31–39 (Coatings for Corrosion Protection).
[5] S. Sharifi Golru, M.M. Attar, B. Ramezanzadeh, Effects of different surface cleaning procedures on the superficial morphology and the adhesive strength of epoxy coating on aluminium alloy 1050, Prog. Org. Coat. 87 (2015) 52–60.
[6] H. Ishida, D. Allen, Physical and mechanical characterization of near-zero shrinkage poly benzoxazines, J. Polym. Sci. B: Polym. Phys. 34 (1996) 1019–1030.
[7] M.C. Tseng, Y.L. Liu, Self-assembled benzoxazine-bridged polysilsesquioxanes exhibiting ultralow-dielectric constants and yellow-light photoluminescent emission, Polymer 51 (2010) 5567–5565.
[8] J. Escobar, M. Poorteman, L. Dumas, L. Bonnaud, Ph. Dubois, M.-G. Olivier, Thermal curing study of Bisphenol A benzoxazine for barrier coating applications on 1050 aluminum alloy-, Prog. Org. Coat. 70 (2013) 53–61.
[9] M. Poorteman, A. Renaud, J. Escobar, L. Dumas, L. Bonnaud, P. Dubois, M.-G. Olivier, Thermal curing of para-phenylenediamine benzoxazine for barrier coating applications on 1050 aluminum alloys, Prog. Org. Coat. 97 (2016) 99–109.
[10] H. Ishida, Y. Rodriguez, Curing kinetics of a new benzoxazine-based phenolic resin by differential scanning calorimetry, Polymer 36 (1995) 3151–3158.
[11] N.N. Ghosh, B. Kiskan, Y. Yagci, Polybenzoxazines-new high performance thermosetting resins: synthesis and properties, Prog. Polym. Sci. 32 (2007) 1344–1391.
[12] L. Dumas, L. Bonnaud, M.-G. Olivier, M. Poorteman, Ph. Dubois, Facile preparation of a novel high performance benzoxazine-CNT based nano-hybrid network exhibiting outstanding thermo-mechanical properties, Chem. Commun. 49 (2013) 9543–9545.
[13] L. Dumas, L. Bonnaud, M.-G. Olivier, M. Poorteman, Ph. Dubois, High performance benzoxazine/CNT nanohybrid network - an easy and scalable way to combine attractive properties, Eur. Polym. J. 58 (2014) 218–225.
[14] F. Keller, M.S. Hunter, D.L. Robinson, Structural features of oxide coatings on aluminum, J. Electrochem. Soc. 100 (1953) 411–419.
[15] G.E. Thompson, Porous anodic alumina: fabrication, characterization and applications, Thin Solid Films 297 (1997) 192–201.
[16] L. Iglesias-Rubianes, S.J. Garcia-Vergara, P. Skeldon, G.E. Thompson, J. Ferguson, M. Beneke, Cyclic oxidation processes during anodizing of Al-Cu alloys, Electrochim. Acta 52 (24) (2007) 7148–7157.
[17] F. Mansfeld, M.W. Kendig, Evaluation of anodized aluminum surfaces with electrochemical impedance spectroscopy, J. Electrochem. Soc. 135 (1988) 828–833.
[18] E. Harscoet, D. Froelich, Use of LCA to evaluate the environmental benefits of substituting chromic acid anodizing (CAA), J. Clean. Prod. 16 (2008) 1294–1305.
[19] G.D. Sulka, K.G. Parkoła, Temperature influence on well-ordered nanopore structures grown by anodization of aluminium in sulphuric acid, Electrochim. Acta 52 (2007) 1880–1888.
[20] G. Boisier, N. Pébère, C. Druez, M. Villatte, S. Suel, FESEM and EIS study of sealed AA2024 T3 anodized in sulfuric acid electrolytes: influence of tartaric acid, J. Electrochem. Soc. 155 (2008) C521–C529.
[21] L. Domingues, J.C.S. Fernandes, M. Da Cunha Belo, M.G.S. Ferreira, L. Guerra-Rosa, Anodising of Al 2024-T3 in a modified sulphuric acid/boric acid bath for aeronautical applications, Corros. Sci. 45 (2002) 149–160.
[22] A. Viola (MESSIER BUGATTI), Anodisation process of an aluminium alloy element, European Patent 1357206 (A2) (2003).
[23] M. Curioni, P. Skeldon, E. Koroleva, G.E. Thompson, J. Ferguson, Role of tartaric acid on the anodizing and corrosion behavior of AA 2024 T3 aluminum alloy, J. Electrochem. Soc. 56 (4) (2009) C147–C153.
[24] A. Dattilo, S. Tamiro, C. Romano (ALENIA AERONAUTICA S.P.A.), Anodizing process, with low environmental impact, for a workpiece of aluminium or aluminium alloys, European Patent EP1233084 (A2) (2002).
[25] S.A Sonaca, Gosselies-Belgium. Process Specification - Tartaric Sulphuric Anodizing of Aluminium Alloys. SONACA - P.S.N°6.5507 (2013).
[26] P. Shulman, A.J. Bauman, Organic acid sealants for anodized aluminum – a new method for corrosion protection, Metal Finish. 93 (7) (1995) 16–19.
[27] K. Bonnel, C. le Pen, N. Pébère, E.I.S. characterization of protective coatings on aluminum alloys, Electrochim. Acta 4 (24) (1999) 4259–4267.
[28] G.C. Wood, V.J.J. Marron, Studies of the sealing of anodized aluminum using alternating current impedance techniques and electron probe microanalysis. I. Sealing in typical salt solutions, Trans. Inst. Met. Finish. 5 (1) (1967) 17–26.
[29] M. García-Rubio, M.P. de Lara, S. Ocón, M. Diekhoff, A. Lavía, I. García, Effect of postreatment on the corrosion behaviour of tartaric-sulphuric anodicfilm, Electrochim. Acta 54 (2009) 4789–4800.
[30] A. Bautista, J.A. Gonzalez, V. Lopez, Influence of triethanolamine additions on the sealing mechanism of anodized aluminium, Surf. Coat. Technol. 154 (2002) 49–54.
[31] X. Yu, Study of the rare earth sealing procedure of the porous film of anodized 2024 aluminum alloy, J. Mater. Sci. Technol. 9 (1) (2003) 51–53.
[32] C.M. Rangel, M.A. Travassos, Alternative chromium free sealant anodizing procedure using lithium ions, ATB Metall. 37 (2-3-4) (1997) 184–187.
[33] H.A. Katzman, G.M. Malouf, R. Bauer, G.W. Stupian, Corrosion-protective chromate coatings on aluminum, Appl. Surf. Sci. 2 (1979) 416–432.
[34] A.-P. Romano, M. Fedel, F. Deflorian, M.-G. Olivier, Silane sol-gel film as pretreatment for improvement of barrier properties and filiform corrosion resistance of 6016 aluminium alloy covered by cataphoretic coating, Prog. Org. Coat. 72 (2011) 695–702.
[35] J.B. Bajat, I. Milošev, Ž. Jovanović, R.M. Jančić-Heinemann, M. Dimitrijević, V.B. Mišković-Stanković, Corrosion protection of aluminium pretreated by vinyltriethoxysilane in sodium chloride solution, Corros. Sci. 52 (3) (2010) 1060–1069.
[36] I. Recloux, M. Debliquy, A. Baroni, Y. Paint, A. Lanzutti, L. Fedrizzi, M.-G. Olivier, Optimization of synthesis parameters of mesoporous silica sol-gel thin films for application on 2024 aluminum alloy substrates, Appl. Surf. Sci. 277 (2013)

201–210.
[37] V.B. Mišković-Stanković, M.R. Stanić, D.M. Dražić, Corrosion protection of aluminium by a cataphoretic epoxy coating, Prog. Org. Coat. 36 (1999) 53–63.
[38] J. Singh-Beemat, J.O. Iroh, L. Feng, Mechanism of corrosion protection of aluminum alloy substrate by hybrid polymer nanocomposite coatings, Prog. Org. Coat. 76 (2013) 1576–1580.
[39] M. Conradi, A. Kocijan, M. Zorko, I. Verpoest, Damage resistance and anticorrosion properties of nanosilica-filled epoxy-resin composite coatings, Prog. Org. Coat. 80 (2015) 20–26.
[40] M. Rashvand, Z. Ranjbar, Effect of nano-ZnO particles on the corrosion resistance of polyurethane-based waterborne coatings immersed in sodium chloride solution via EIS technique, Prog. Org. Coat. 76 (2013) 1413–1417.
[41] F. Snogan, C. Blanc, G. Mankowski, N. Pebere, Characterisation of sealed anodic films on 7050 T74 and 2214 T6 aluminium alloys, Surf. Coat. Technol. 154 (2002) 94–103.
[42] P. Zoltowski, On the electrical capacitance of interfaces exhibiting constant phase element behavior, J. Electroanal. Chem. 443 (1998) 149–154.
[43] F. Deflorian, L. Fedrizzi, Adhesion characterization of protective organic coatings by electrochemical impedance spectroscopy, J. Adhes. Sci. Technol. 13 (5) (1999) 629–645.
[44] E.P.M. van Westing, G.M. Ferrari, J.H.W. de Wit, The determination of coating performance with impedance measurements—III. in situ determination of loss of adhesion, Corros. Sci. 36 (6) (1994) 979–994.
[45] A. Amirudin, D. Thierry, Application of electrochemical impedance spectroscopy to study the degradation of polymer-coated metals, Prog. Org. Coat. 26 (1995) 1–28.
[46] V.R. Capelossia, M. Poelman, I. Recloux, R.P.B. Hernandez, H.G. de Melo, M.G. Olivier, Corrosion protection of clad 2024 aluminum alloy anodized intartaric-sulfuric acid bath and protected with hybrid sol-gel coating, Electrochim. Acta 124 (2014) 69–79.
[47] S.G. Mazzini, J.C. Caretti, Effect of deformation at elevated temperature before age-hardening on the mechanical properties of 2024 commercial aluminium alloy, Scripta Metallurgica et Materialia 25 (8) (1991) 1987–1990.